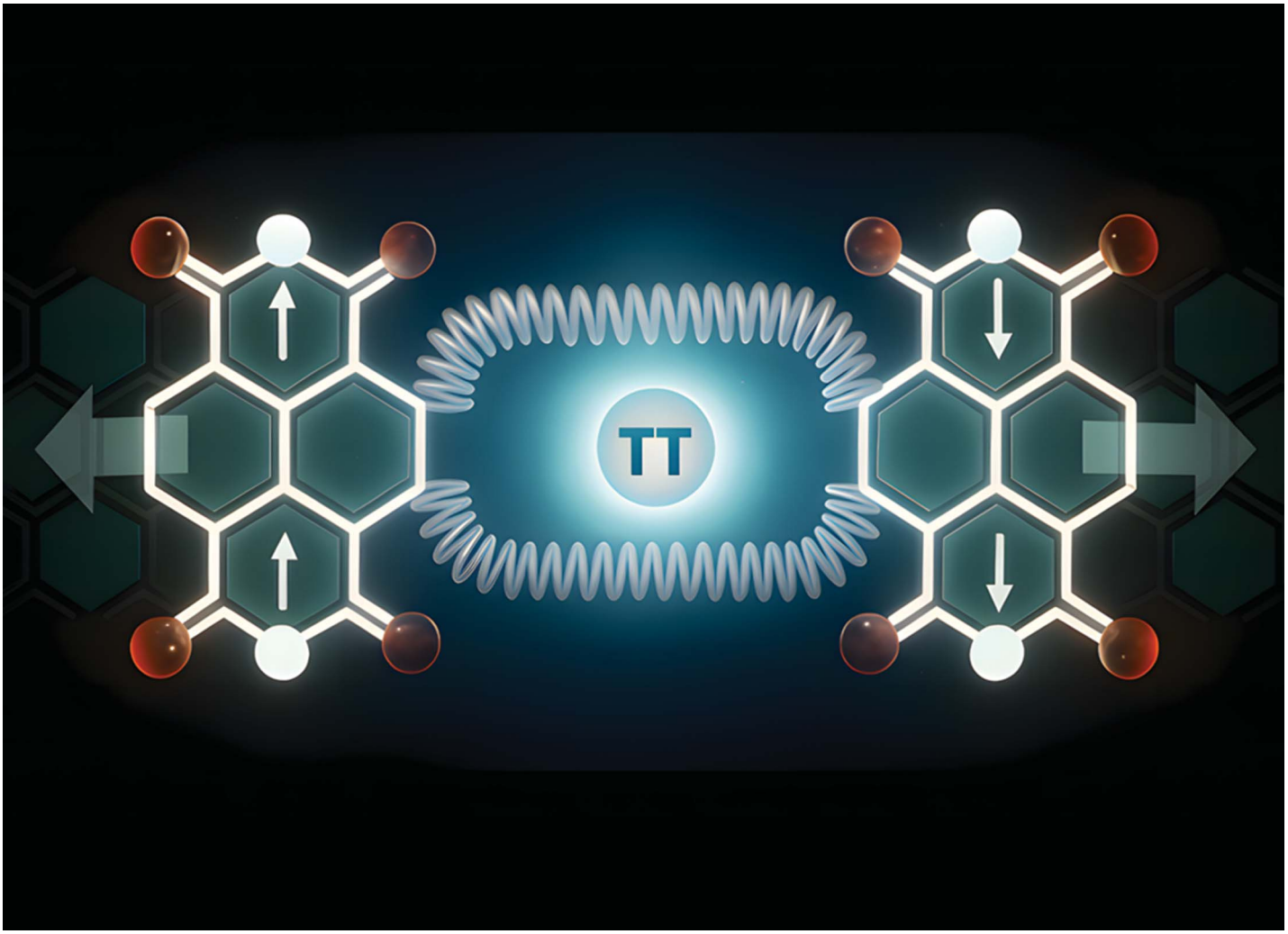

Showcasing the joint collaborative work from the research groups of Professor Jyotishman Dasgupta (TIFR Mumbai), Pritam Mukhopadhayay (JNU New Delhi) and Debashree Ghosh (IACS Kolkata).

An order of magnitude modulation of singlet fission rates in NDI cyclophanes by tuning inter-chromophoric electronic coupling

Through a series of synthetically challenging and structurally well-defined dimeric naphthalene-diimide (NDI) cyclophanes, we demonstrate that ultrafast singlet fission (SF) is dictated by stabilization of the multi-excitonic ^{1}TT pair state on a dimer-backbone rather than the singlet-triplet energetics of its constitutive monomers. Our work highlights that the rates of SF can be tuned by optimal modulation of the inter-chromophoric distance and orientation, parameters that critically define the electronic coupling.

Image reproduced by permission of Aisworika Mohanty from *Chem. Sci.*, 2025, **16**, 21368. Image created with Google Gemini.

As featured in:

See Aisworika Mohanty and Vijay Pal Singh *et al.* *Chem. Sci.*, 2025, **16**, 21368.

ROYAL SOCIETY OF CHEMISTRY

15 YEARS ANNIVERSARY

rsc.li/chemical-science

Registered charity number: 207890

Chemical Science

ROYAL SOCIETY OF CHEMISTRY

EDGE ARTICLE

View Article Online
View Journal | View Issue

Cite this: *Chem. Sci.*, 2025, **16**, 21368

All publication charges for this article have been paid for by the Royal Society of Chemistry

An order of magnitude modulation of singlet fission rates in NDI cyclophanes by tuning inter-chromophoric electronic coupling

Aisworika Mohanty,†[a] Vijay Pal Singh,†[b] Ch. Mudasar Hussain,[b] Mandira Dey,[c] Debashree Ghosh,*[c] Pritam Mukhopadhyay*[b] and Jyotishman Dasgupta*[a]

Received 8th August 2025
Accepted 22nd October 2025

DOI: 10.1039/d5sc05995j

rsc.li/chemical-science

Singlet fission (SF) is a process of multi-exciton generation in molecular aggregates where two independent triplet states are formed *via* an intermediate correlated triplet–triplet ^{1}(TT) pair state. SF has been shown to occur within a minimal dimeric unit with chromophores having monomer triplet energies that are half the allowed bright singlet state energy. However, optimal singlet fission rates can only be derived if structural rules are formulated for tunable interchromophoric coupling between the two monomer units, which has remained a significant challenge in the community. In order to uncover the electronic nature of the dynamic ^{1}(TT) stabilization in generic supramolecular dimeric constructs, herein we have synthesized five new napthalene-diimde (NDI) cyclophanes by altering the distance and angle between the NDI units. Using a combination of transient absorption spectroscopy supported by high-level electronic structure calculations, we find that SF is tolerant in these rigid dimeric structures up to distances of 4.5 Å while the rise of the ^{1}(TT)-state gradually slows down from 400 fs to 4.6 ps concomitant with the decrease in the inter-chromophoric electronic coupling. Our work therefore demonstrates that the thermodynamic criterion of singlet exciton fission isn't in the singlet–triplet energetics of the constitutive monomer but rather in the stabilization of the multiexcitonic ^{1}(TT) pair state in its minimal dimeric unit.

Introduction

Singlet fission (SF), the molecular equivalent of multiple exciton generation, has attracted considerable attention for its potential applications in organic optoelectronic devices. It is a process that can convert a high-energy singlet exciton into two low-energy triplet excitons through an intermediate triplet pair ^{1}(TT) state, first observed in anthracene crystals.[1–3] However, the concept gained significant popularity in 2006 when it was demonstrated to increase the power conversion efficiency of solar cells that could surpass the Shockley–Queisser (SQ) limit.[4,5] Marc Baldo and coworkers incorporated a layer of tetracene into a single-junction silicon solar cell which can theoretically increase the cell efficiencies from the single-junction limit of 29 percent to as high as 35 percent.[6] Apart from photovoltaics, recently, Xiaochen Dong and coworkers have demonstrated a heavy-atom-free (HAF) photosensitizer design strategy founded on the SF mechanism for cancer photodynamic therapy, where the SF process led to an ultrahigh triplet-state quantum yield (186%).[7] Therefore, increasing the

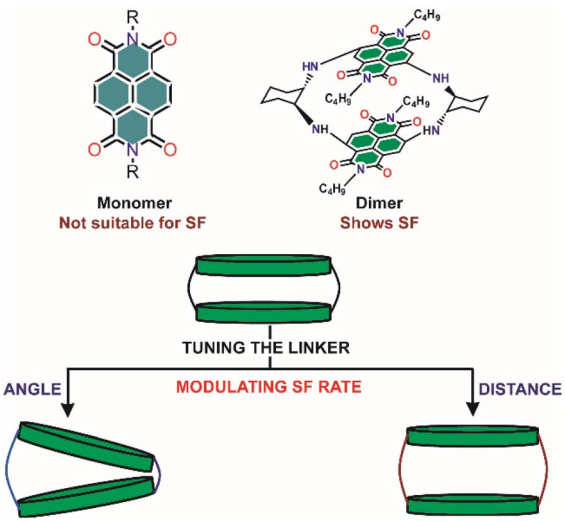

Fig. 1 (Top): schematic representation of the NDI dimer (right) that shows SF although the parent monomer (left) does not satisfy the thermodynamic criteria for SF. (Bottom): tuning of the inter-chromophoric coupling by increasing the separation *via* symmetric linkers or by opening up the inter-chromophoric angles *via* unsymmetric linkers.

[a]*Department of Chemical Sciences, Tata Institute of Fundamental Research, Homi Bhabha Road, 400005, India. E-mail: dasgupta@tifr.res.in*

[b]*School of Physical Sciences, Jawaharlal Nehru University, New Delhi 110067, India. E-mail: m_pritam@mail.jnu.ac.in*

[c]*School of Chemical Sciences, Indian Association for the Cultivation of Science, Kolkata, 700032, West Bengal, India. E-mail: pcdg@iacs.res.in*

† A. M. and V. P. S. contributed equally to this work.

efficiency of this multiple-exciton generation as well as understanding the behavior of these triplet excited states formed by SF is crucial for developing strategies to design practically applicable SF chromophores.[8–10]

The mechanistic investigations of functional singlet fission processes have been elucidated in films of molecular aggregates in the solid-state using a variety of spectroscopic and imaging studies to elaborate the so-called inter-molecular SF process.[11] Crucial insights into the mechanism of SF have also been gained recently from observations of intra-molecular SF in covalently bound dimeric and/or multimeric constructs of chromophores.[12–15] Unlike the difficulties in controlling the morphology of self-assembling molecular solids/aggregates, the relative chromophoric orientations in such dimeric systems can be homogeneously controlled through careful linker designs. In 2015, Campos and co-workers showed that the degree of electronic coupling between covalently bound pentacene molecules in a molecular dimer determines the fission rate and consequent triplet lifespan.[16] However, it was also noted recently that open acyclic dimers with flexible linkers undergoing SF often have rate dispersion due to conformational flexibility in the ground state.[17–19] Patil, Musser and coworkers explored the SF dynamics of the pentacene dimer linked by phenyldiketopyrrolopyrrole and acetylene bridges, and they could observe a heterogeneous rate of SF due to the unrestricted rotations that yield a myriad of rotational conformers, each altering the SF processes.[20] Such distribution makes it difficult to understand mechanistic details due to the dispersion in SF rates for different inter-chromophoric distances and torsional angles.[21]

Rigid cyclophanes in contrast, although synthetically challenging, provide a tunable framework to elaborate the distance and orientation dependence in SF rates.[22] Utilizing this idea, Yanai and coworkers have recently synthesized a pentacene based macrocyclic parallel dimer where the macrocyclic structure keeps the pentacene units oriented parallel to each other in close proximity in solution or a polymer matrix, leading to ultrafast SF of less than 100 fs and allowing the selective population of specific quintet sublevels at room temperature.[23] Recently, Bansal and Kundu *et al.* designed the first example of a naphthalene di-imide (NDI) dimer, in a rigid cyclophane framework. Due to strong electronic coupling between the two NDI units, the dimer showed SF, although the monomer doesn't fulfil the energy criteria. In fact, the work strongly indicates that the presence of an energy-stabilized multi-excitonic ^{1}(TT) state (ME) is the only necessary criterion for SF in any minimalist dimer, thereby eliminating the need for chromophores with appropriate thermodynamics of singlet and triplet states.[24] Therefore, in order to test the geometric limits of ME state stabilization on the parent NDI dimer backbone, it is imperative to synthesize supramolecular NDI constructs with a variety of distances and chromophoric orientations as shown in Fig. 1.

Herein, we synthesized five new NDI cyclophane structures with rigid control over inter-chromophoric distances and angles to understand the efficiency of ME generation systematically, inspired by the classic work of Stryer and Haugland on the FRET process.[25] The cylcohexyldiamine linkers for the *Cyclo-Cyclo* (Push–Pull NDI Dimer, PPD) provided a NDI center-to-center distance of ~3.3 Å between the two NDI units. In order to increase the inter-chromophoric distances, here we installed *ortho*- and *meta*-substituted xylylene diamine linkers, while angular changes were made by installing xylylene diamine linkers in combination with the cyclohexyl diamine linkers. The systematic weakening of inter-chromophoric coupling *via* distance expansion or angular rotation led to our observation of slowing down the ^{1}(TT) state formation timescale through broadband femtosecond transient absorption spectroscopy. Quantifying the coupling strength using electronic structure calculations provided further insight into the energy of the ME state and its dependence on distance/orientations.

Results

Design, synthesis and structural parameters of the cyclophanes

The NDI cyclophane (*Cyclo-Cyclo*)[11] was the first example of a co-facial push–pull construct with an interchromophoric distance of 3.3 Å. The short and rigid cyclohexyldiamine linker ensured a strong electronic coupling along with a highly distorted π-backbone of the NDI monomers. Following the reported protocol for the synthesis of the *Cyclo-Cyclo*, in this work we synthesized two symmetric dimers with *ortho*-and *meta*-substituted xylylenediamine linkers named as *Ortho-Ortho* and *Meta-Meta* cyclophanes. Additionally, in order to tune the angles between the chromophores, we synthesized three unsymmetric dimers by installing cyclohexyldiamine linkers with either *o*-/*m*-xylylenediamine linkers resulting in *Cyclo-Ortho*, *Cyclo-Meta* and *Ortho-Meta* NDI cyclophanes.

The symmetric NDI cyclophanes (*Ortho-Ortho*, *Meta-Meta*) were synthesized from the corresponding *Ortho* Clip and *Meta* Clip by reacting with *o*-xylylene diamine/*m*-xylylene diamine, respectively, in *p*-dioxane under inert conditions (Scheme 1, SI). On the other hand, unsymmetric NDI cyclophanes (*Cyclo-Ortho*, *Cyclo-Meta*, and *Ortho-Meta*) were synthesized from the *Ortho* Clip, *Cyclo* Clip and *Ortho* Clip by reacting with *R*,*R*-trans-1,2-cyclohexyldiamine/*m*-xylylenediamine/*m*-xylylenediamine, respectively, in *p*-dioxane under inert conditions (Scheme 2, SI). The yields of the cyclophanes ranged between 5-10%. The second ArS_N reaction on the preorganized *Cyclo*/*Ortho*/*Meta* Clips for the macrocyclization is challenging considering the electronic factors, which impacts the yield of the isolated cyclophanes. The synthesized compounds were characterized by various spectroscopic techniques and in a few cases by single-crystal X-ray crystallography. Interestingly, ^{1}H NMR analysis disclosed distinct chemical shifts in the symmetric and unsymmetric cyclophanes (Fig. S1–S9). In the *Ortho-Ortho* cyclophane, the NDI H's appear at 7.80 ppm, which are shielded by 0.09 and 0.1 ppm compared to the *Meta-Meta* and *Cyclo-Cyclo* cyclophanes. Likewise, the NH protons which appear at 9.27 ppm in *Ortho-Ortho* are shielded by 0.14 and 0.51 ppm with respect to the Cyclo-Cyclo and *Meta-Meta* cyclophanes. In the case of the unsymmetric cyclophanes, the NDI H's of *Cyclo-Ortho* cyclophane appear at 7.87 and 7.76 ppm, those of the *Cyclo-Meta* at 8.17 and 7.74 ppm, and those of *Ortho-Meta*

cyclophane at 7.97 and 7.75 ppm. This clearly showed that the *m*-xylylene diamine and the cyclohexyl diamine linkers can position the NDI chromophores at the closest possible distance.

We successfully crystallized one of the symmetric *Meta-Meta* dimers along with an unsymmetric *Ortho-Meta* dimer, thereby comparing the geometric parameters to the original *Cyclo-Cyclo* dimer. For the symmetric dimer, we find that the center-to-center interchromophoric distance is increased to 3.920 Å as compared to the *Cyclo-Cyclo* derivative. From the crystal structures, we could observe a distorted backbone in case of the *Cyclo-Cyclo* derivative having the central region arched outwards, whereas in the *Meta-Meta* derivative, the central part has a concave type geometry having an inwardly arched backbone. This is in contrast to the unsymmetric dimer geometry where we observe clear changes in the inter-chromophoric angles. For the unsymmetric linkers, the opening at one end of the cyclophane structure is comparatively wider than the other.

In case of the *Cyclo-Cyclo* derivative, the C atoms make the shortest contacts of 3.084(1) Å and 3.128(1) Å, respectively. As we increased the linker length from cyclohexyl diamine to xylylene diamine, we observed an inwardly arched backbone in case of the *Meta-Meta* dimer. The crystal structure clearly showed an increase of the C2–C3 distance from 3.084 Å and 3.128 Å (*Cyclo-Cyclo*) to 4.059(9) Å (*Meta-Meta*). However, in the case of *Ortho-Meta*, the unsymmetrical linker led to a longer C2–C3 distance of 4.712(1) Å at one end as compared to the other end (3.453(2) Å). The non-eclipsed stacking arrangement of the two π-

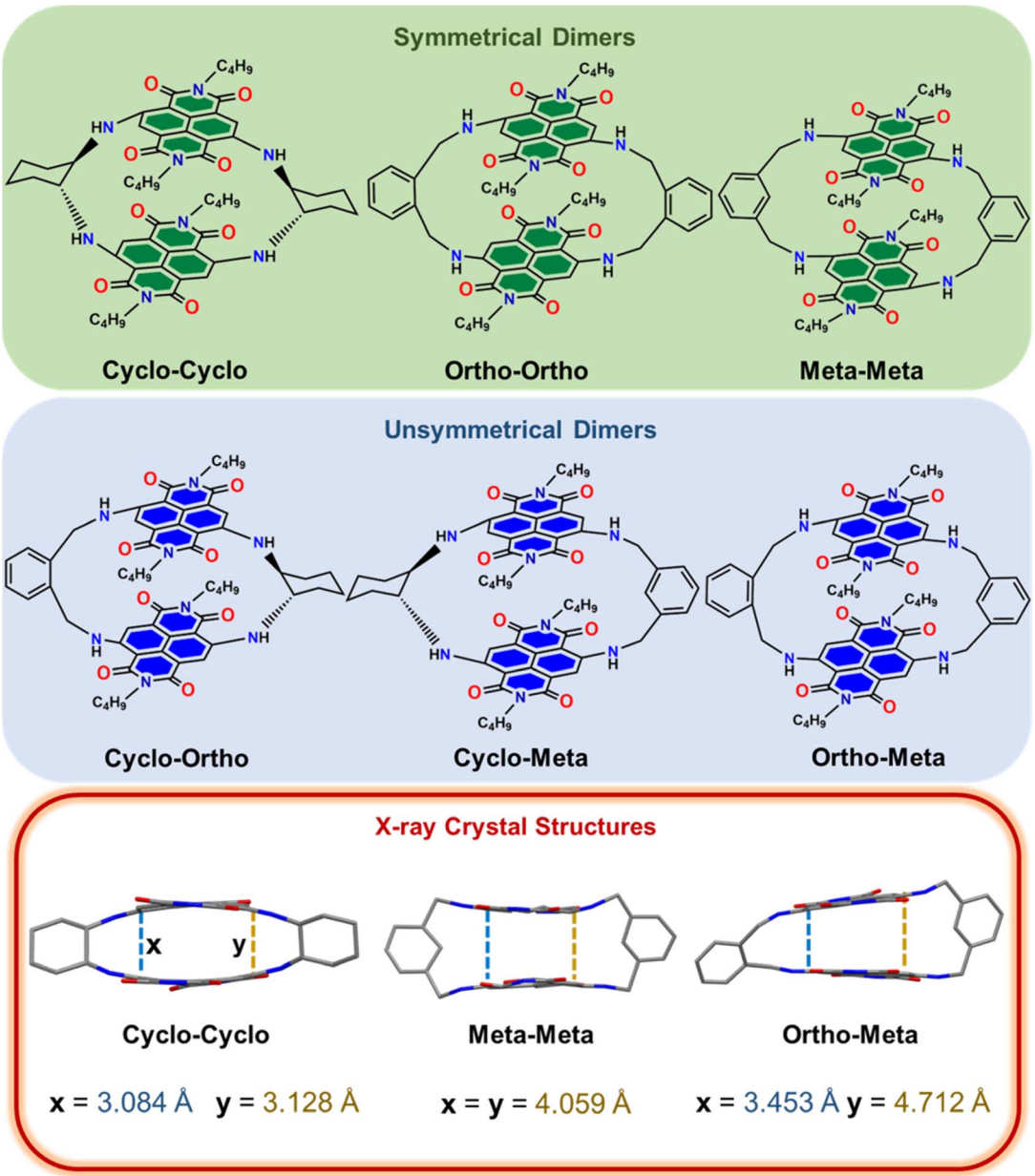

Scheme 1 Schematic representation of the previously reported *Cyclo-Cyclo* dimer and the new dimers presented in this work with varying interchromophoric distance and orientation, along with the crystal structure (side view) of Cyclo-Cyclo, *Meta-Meta* and *Ortho-Meta* dimers.

surfaces in case of the *Cyclo-Cyclo* dimer leads to a twist by 20° and 24° along the long- and short-axes, respectively. In the *Meta-Meta* derivative, there is no significant twisting along the long-axis as well as along the short-axis. The unsymmetrical *Ortho-Meta* derivative also had a twisted backbone having a torsional angle of 22° along the long axis and 11° along the short axis. These crystal structures suggest that by linking the chromophores along the short axis, we could actually induce a greater contortion in this dimeric backbone (Scheme 1).

Optical spectroscopy of the dimers

In order to understand the electronic coupling in the dimers, we carried out steady state absorption spectroscopy. The absorption spectrum of the NDI monomer exhibits bands in the regions 325–420 and 440–660 nm corresponding to π–π* and ICT transitions, respectively (Fig. 2). However, the *Cyclo-Cyclo* dimer, having the closest interchromophoric distance, shows a significantly broadened absorption band ($FWHM_{ICT}$ = 3633 cm^{-1}) at 630 nm as compared to that of the monomer ($FWHM_{ICT}$ = 2147 cm^{-1}). In addition, a 112 cm^{-1} red-shift is observed in the absorption maximum as reported previously. Apart from the broadening, there is a decrease in molar absorption coefficient in case of the dimer as compared to the monomer which suggests the presence of strong electronic coupling between the two stacked monomeric units.

In case of the symmetric dimers, the *Ortho-Ortho* and *Meta-Meta* dimers show narrower absorption features having peak maxima at 596 and 606 nm, respectively. Although these absorption bands are narrower than those of the original *Cyclo-Cyclo* dimer, this is still broader as compared to the monomer with FWHM values of 2190 and 2219 cm^{-1}. But we did not observe any significant red shifting in case of the *Ortho-Ortho* dimer. The *Meta-Meta* dimer however has a 277 cm^{-1} red shift compared to the ICT absorption feature in the monomer. The unsymmetrical dimers show absorption features with maxima at 610, 612 and 621 nm for *Ortho-Meta*, *Cyclo-Meta* and *Cyclo-Ortho*, respectively. These showed a broader ICT band as compared to the symmetrical ones, having FWHM values of 2706, 2430 and 2282 cm^{-1} for the *Cyclo-Ortho*, *Cyclo-Meta* and *Ortho-Meta* dimers, respectively. Also, these unsymmetrical dimers showed a significantly red shifted ICT band which was quantified to be 676, 439 and 399 cm^{-1} in case of *Cyclo-Ortho*, *Cyclo-Meta* and *Ortho-Meta* dimers, respectively (Fig. S15). The lesser broadening in all these new dimers indirectly indicates that the *Cyclo-Cyclo* derivative has the strongest interchromophoric interaction among all. However, the red shifted absorption band in the new dimers still shows the presence of interchromophoric interactions with varying coupling strength. The values of the FWHM as well as the redshift for all the dimers have been tabulated in the SI (Table S1). This comparative study of the absorption spectra indicated that upon increasing the linker length, we could actually change the interchromophoric coupling in these dimers.

We carried out steady state emission measurements for all the dimers to appreciate ultrafast excited state deactivation channels. In fact, all dimers showed a quenched fluorescence upon 540 nm excitation, as compared to the monomer (Fig. S16). As the emission arises from the S_1 state and in all the dimers the fluorescence is quenched, this indicates that the S_1 state is involved in some non-radiative processes which are absent in the monomer. The monomer showed an intense fluorescence spectrum having a peak maximum at 628 nm. However, in case of the dimers, not only is the emission quenched but also the spectral feature is distinct from that of the monomer. This indicates that the quenched emission arises from some other relaxed state, ^{1}(TT), and not from the S_1 state. Although ^{1}(TT) is potentially a dark state, it can however borrow some oscillator strength from the neighbouring bright S_1 state if there is strong electronic coupling with the ^{1}(TT) state to give rise to a partially quenched emission. *Cyclo-Ortho*, *Meta-Meta* and *Ortho-Ortho* showed an emission feature characterized by peak maxima in the range 570–580 nm and 640–660 nm. However, in case of both *Ortho-Meta* and *Cyclo-Meta*, we

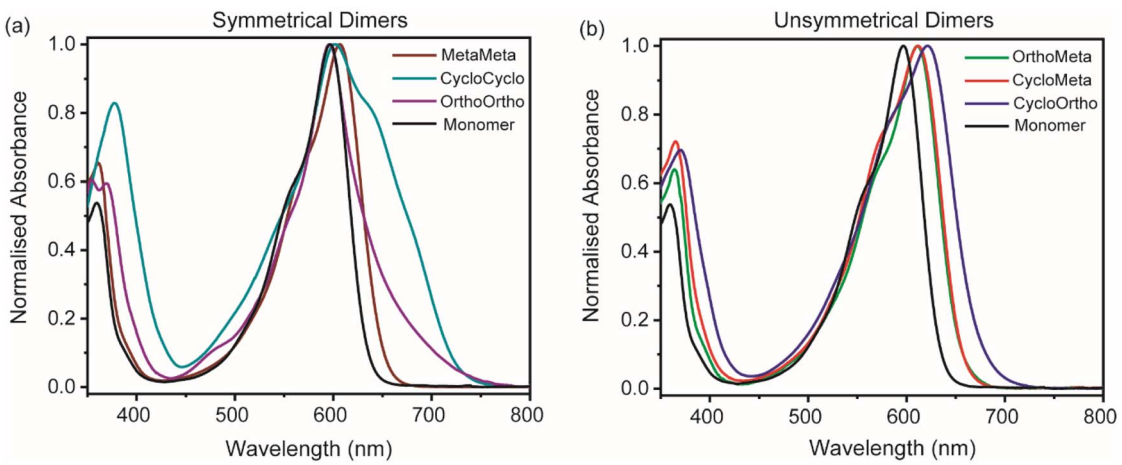

Fig. 2 Normalized steady state absorption spectra of (a) symmetrical and (b) unsymmetrical dimers along with the corresponding monomer. The *Ortho-Meta* spectrum in the unsymmetrical dimers plot is buried under the *Cyclo-Meta* case. All the dimers show electronic coupling between the NDI units with varying coupling strength.

observed an emission spectrum, having single peak maxima in the region 670–680 nm. It should be noted here that for the *Cyclo-Cyclo* derivative, the emission spectra were weak and difficult to resolve compared to those of the other dimers.

In order understand if this is dynamic quenching of the excited states, we carried out time-correlated single photon counting (TCSPC) measurement by exciting the samples at 295 nm with an IRF of ~100 ps. The TCSPC data for the monomer was fitted to a single exponent, which gave rise to a lifetime of ~13 ns. However, for all the dimers, a three-component model has been used. When we calculated the amplitude-weighted average lifetime, it clearly showed a quenched lifetime of 240 ps (*Cyclo-Cyclo*), 2.1 ns (*Cyclo-Ortho*), 2.3 ns (*Cyclo-Meta*), 3.4 ns (*Ortho-Ortho*), 1.6 ns (*Ortho-Meta*), and 366 ps (*Meta-Meta*) as compared to the monomer (Fig. S17). From the previous study on the *Cyclo-Cyclo* dimer, we could obtain indirect proof that this fluorescence lifetime quenching can be due to the ultrafast SF process occurring in these dimers. So, our next goal was to check if SF is indeed happening by probing the excited state dynamics and see how the change in the interchromophoric interaction will affect the SF dynamics.

Femtosecond broadband transient absorption spectroscopy

To get a deeper insight into the excited state dynamics, we performed fs–ns transient absorption (TA) spectroscopy. The excited state dynamics of these dimers were probed using a broadband white light continuum (430–1300 nm) after 400 nm femtosecond pump excitation in a 1 : 1 mixture of ACN and DCM. Fig. 3a shows the TA data of *Cyclo-Ortho* and *Meta-Meta* dimers with a time delay from −370 fs up to 2 ns in the spectral range of 450 to 750 nm. After excitation, we could see two excited state absorption (ESA) features ranging from 450–550 and 650–750 nm along with a negative ground state bleach (GSB) feature resembling the ICT band of the ground state absorption spectra. However, the ESA peak maximum in case of the *Meta-Meta* dimer is slightly red shifted (~278 cm^{-1}) as compared to that of the *Cyclo-Ortho* derivative. These features completely decay within tens of picoseconds. Similar features were also observed in the case of *Cyclo-Meta*, *Ortho-Ortho* and *Ortho-Meta* derivatives (Fig. S18). To get an idea about the timescales of the evolution of these features, we performed single-point kinetic data fitting with a two-state sequential model. In case of the *Cyclo-Ortho* dimer, first there is a rise of a component in 620 fs followed by a mono-exponential decay of 49 ps. In contrast, in case of the *Meta-Meta* dimer having the weakest interchromophoric interaction, the first component slowly rises in 4.5 ps followed by two decaying components having a lifetime of 34 and 115 ps, respectively (Fig. S23). When we performed the single point kinetic fitting at both the ESA and GSB features, we could observe that the rise of the GSB is accompanied by the appearance of a new excited state feature within similar timescales. This is indirect proof of SF because the S_0S_1 interaction leads to the formation of a new state, most probably ^{1}(TT), within a similar timescale (Fig. S20).

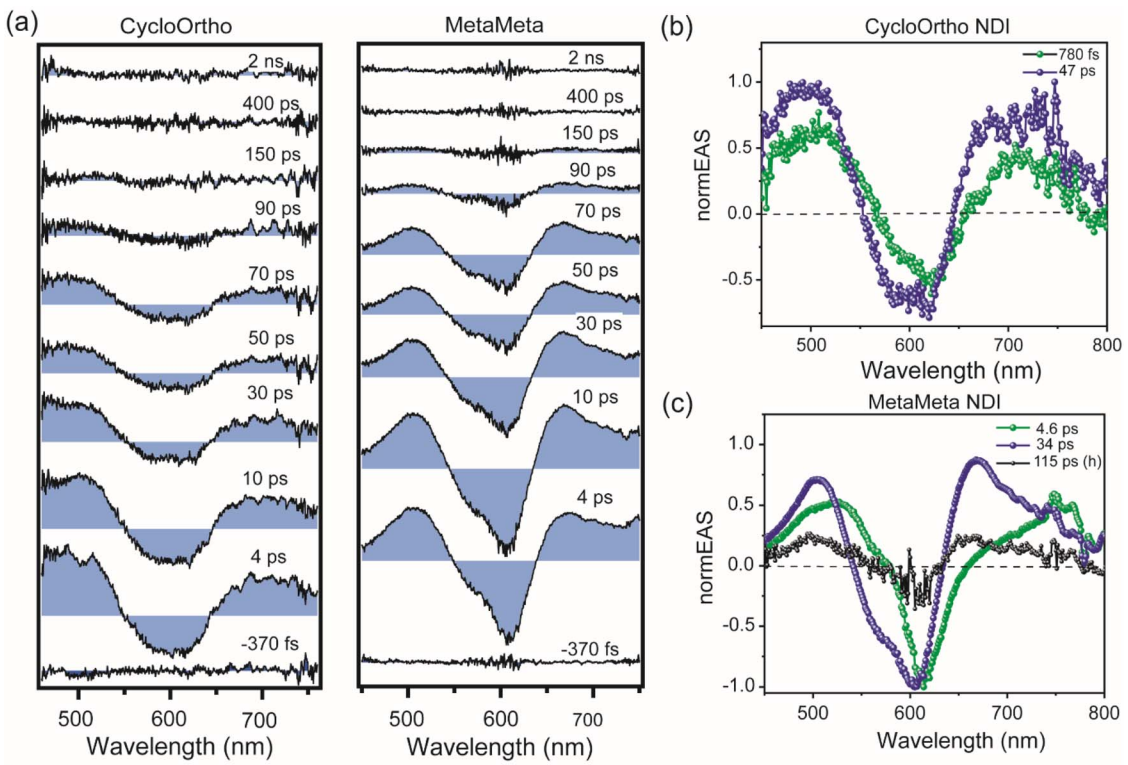

Fig. 3 (a) fs–ns TA spectra of 400 μM *Cyclo-Ortho* and 200 μM *Meta-Meta* dimers in ACN: DCM (1 : 1) upon photoexcitation at 400 nm with a time delay from −370 fs to 2 ns. Two and three state sequential singular value decomposition of the TA spectra of (b) *Cyclo-Ortho* and (c) *Meta-Meta* dimers, respectively. We have also done the measurement on 200 μM *Cyclo-Ortho* which shows similar dynamics.

Subsequently, we performed multi-wavelength global analysis using singular value decomposition (SVD) (Fig. 3b and c) to resolve all the components in the TA spectra along with their lifetimes. For the *Cyclo-Ortho* dimer, we used a two-state sequential model. The first component, attributed to the S_1 state, has a lifetime of 780 fs followed by the second decaying component having a lifetime of 47 ps. However, in case of the *Meta-Meta* derivative, we had to use a three-state sequential model. The initial component has a longer lifetime of around 4.6 ps as compared to the *Cyclo-Ortho* derivative, followed by two decaying components with 34 and 115 ps lifetime. We have performed the SVD analysis for the other dimers as well, which have been shown in Fig. S21 and S23. In all of them, we could fit the data with a two-state sequential model unlike the *Meta-Meta* dimer where we observed a slightly blue-shifted third component.

In order to probe any heterogeneity in SF rates, we carried out excitation wavelength dependent transient absorption measurements. For this we excited one of the dimers (*Cyclo-Meta*) at 600 nm. The excited state features were similar to the features that we got after 400 nm excitation with no significant change in the lifetimes (Fig. S24 and S25). Further, to rule out that the excited state features are arising from the dimeric system and not the monomeric unit, we performed the TA measurements on the NDI monomer (Fig. S26–S30). Upon photoexcitation at 400 nm, first there was formation of two ESA and one GSB feature. With time, the initial ESA feature evolves into a new double-hump ESA feature in the singlet manifold that lives up to >2 ns.The multiwavelength SVD analysis was done using a two-state sequential model. The first component, having a peak maximum at 500 nm, had a lifetime of 1.4 ps followed by the long-lived double hump feature. When we compared this data to that of the dimer, we concluded that the initial feature in case of the dimers corresponds to the singlet state. However, the spectral feature of the second component, in case of the dimer, is completely different from that of the monomer with a shorter lifetime of tens of ps whereas the monomeric feature lives up to >2 ns. Hence, it was concluded that in case of the dimers, the second component is getting formed due to some other photophysical process. To characterize the second component formed in all these dimers, we looked back at the reported spectral feature for the ^{1}(TT) intermediate in case of the *Cyclo-Cyclo* dimer, which was confirmed *via* the sensitization process (Fig. S31). When we compared the spectral features of all these new dimers, we could predict the formation of ^{1}(TT) in all these dimers *via* SF (Fig. S21).

However, to further confirm this process, we performed sensitization in one of the new dimers, *i.e. Cyclo-Meta*. The TA data of the sensitizer, $[Ru\text{-}tris(bipy)_3]^{2+}$-complex, upon 400 nm excitation shows a GSB feature in the 450–500 nm region along with a broad ESA feature ranging from 500–800 nm (Fig. S32 and S33). But when we excited a mixture of *Cyclo-Meta* dimer and the sensitizer (1 : 2) at 400 nm, the features in the fs-ns regime were a convolution of both the dimer and sensitizer features in the initial time points (Fig. S34). After tens of picoseconds, when the dimer features decayed completely, we could clearly observe only the sensitizer features for >2 ns. Then we tracked the dynamics in the ns–μs regime. When there was no dimer mixed with the sensitizer, the features of the sensitizer were clearly decaying within 830 ns (Fig. S33). But for the mixture of the dimer and sensitizer, first there was a decay of the sensitizer feature in 250 ns followed by the rise of a new feature having a lifetime of 4.80 μs *via* sensitization (Fig. 4). The Ruthenium bipyridine complexes are well-known triplet sensitizers. We have performed oxygen-dependent studies in order to confirm the broad ESA feature to be that of a triplet in case of the sensitizer (Fig. S33). In the sensitization process, this triplet energy gets transferred non-radiatively to the *Cyclo-Meta* dimer (rate = 0.004 ns^{-1}) to give rise to the triplets of the *Cyclo-Meta* dimer having a lifetime of 4.8 μs. When we compared the triplet features of the *Cyclo-Meta* dimer to the component that we got

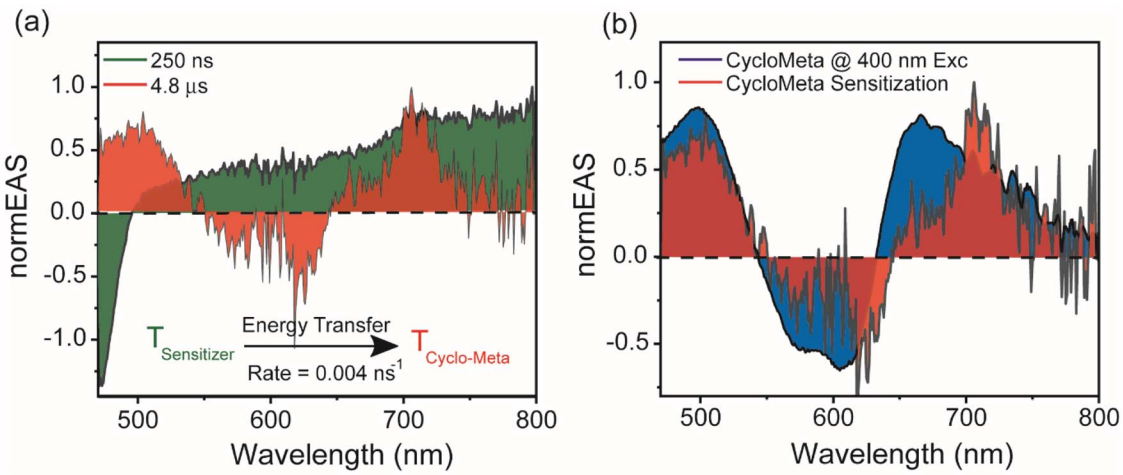

Fig. 4 (a) Two-state sequential singular value decomposition of the ns-μs TA spectra of the triplet sensitization measurement of 200 μM *Cyclo-Meta* dimer with $[Ru\text{-}tris(bipy)_3]^{2+}$-complex (1 : 2) in ACN: DCM (1 : 1) upon photoexcitation at 400 nm, (b) comparative plot of the dimer sensitized data to that of the 50.6 ps component after 400 nm direct excitation.

after direct excitation at 400 nm, the feature of the second component (50.6 ps) matches quite well with that of the triplet (Fig. 4). Hence, we could confirm the formation of a ^{1}(TT) pair intermediate in the *Cyclo-Meta* dimer.

To summarize, after exciting the dimers at 400 nm there is a rise of a new excited state which we have assigned to be the multi-excitonic ^{1}(TT) state. Then, the strong interchromophoric coupling leads to the recombination of the ^{1}(TT) intermediate to the ground state, which has been depicted in Fig. 5a. Interestingly, in case of the *Meta-Meta* dimer, this ^{1}(TT) pair intermediate evolves into a blue-shifted component. Such behavior can only be observed if the ^{1}(TT) pair is relaxing or partially dissociating into a different, more relaxed species. As the generation of completely free triplets in this cyclophane framework is highly unlikely, we have assigned the observed feature to a relaxed ^{1}(T···T) state. The weakest electronic coupling (107 meV) could be the reason for the formation of this slightly separated ^{1}(T···T) pair state in the *Meta-Meta* dimer which was not possible in case of the other dimers. Relaxation to the ^{1}(T···T) species might involve structural rearrangement due to the relatively flexible backbone of the *Meta-Meta* dimer. This can weaken the coupling to S_1 (for borrowing brightness), inducing a faster non-radiative decay pathway. This could be the reason for the shorter emission lifetime (366 ps) observed in the TCSPC measurement for the *Meta-Meta* dimer even after having the longest interchromophoric distance. After SF is confirmed to be occurring in all these dimers, we compared the dynamics of the rate of formation and recombination of ^{1}(TT). As we move from the *Cyclo-Cyclo* dimer having the strongest interchromophoric interaction to the *Meta-Meta* dimer with the weakest interaction, the rate of formation of ^{1}(TT) slowed down from 380 fs to around 4.6 ps. These rates indicate a clear distance-dependent change which goes with an $\sim r^{-12}$ dependence. Interestingly such a dependence possibly implicates short-range repulsion to be a dominant mechanism for controlling SF rates although this needs to be tested more rigorously in future.

Fig. 5b and c clearly shows this trend in both symmetrical and unsymmetrical dimers. This indicates that strong interchromophoric interaction plays a crucial role in the formation of ^{1}(TT). For the symmetrical dimers, the maximum recombination timescale is ~115 ps for *Meta-Meta* while for the other two dimers it is 110 ps (*Ortho-Ortho*) and 70 ps (*Cyclo-Cyclo*), respectively. As the coupling gets weaker from the *Cyclo-Cyclo* to *Meta-Meta* dimer, the ^{1}(TT) pair intermediate is expected to live longer which we observe in case of these symmetric dimers (Fig. 5). However, the rate of recombination of the ^{1}(TT), in the case of unsymmetrical dimers, doesn't follow the systematic changes done on the backbone exemplified by the ground state geometry especially in either distance or inter-chromophoric angles and the range of timescales fall in a narrow window between ~40 and ~50 ps (Fig. 5).

Previous work by Tilley's group had enumerated that molecular dimers can show distance independent ^{1}(TT) recombination rates.[22] In addition, recently, Akshay Rao and coworkers have shown that close coupling is primarily important to ensure efficient triplet generation rather than efficient triplet energy transfer, which is a distance independent process.[26] This indicates a clear role for tracking the excited state geometry change in the ^{1}(TT) state in case of the unsymmetric dimers which may now not directly be correlated to the initial GS geometries. Using ultrafast vibrational techniques, Frontiera and coworkers have tracked the structural evolution during the SF process. They could observe excited state vibrational features that are shifted as compared to the ground state which are indicative of the geometry change in the excited

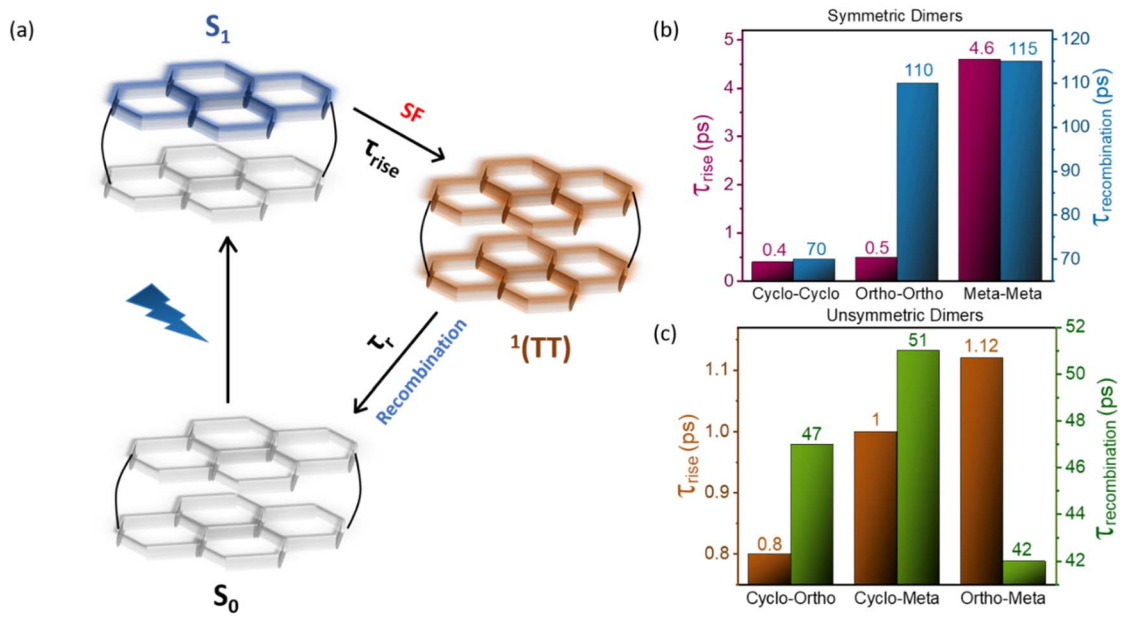

Fig. 5 (a) Energy level diagram summarizing the mechanism of SF and the effect of interchromophoric distance on the rate of formation and recombination of ^{1}(TT). Bar plots showing the trend of τ_{rise} (rate of formation of ^{1}(TT)) and τ_{recomb} (rate of recombination of ^{1}(TT)) with increasing linker lengths in (b) symmetrical and (c) unsymmetrical dimers.

state.[27] It is imperative therefore to understand how excited state geometries contribute to the reaction coordinates that enable recombination of the ^{1}(TT) intermediate which is hard to predict currently for these unsymmetric dimers due to an additional angular variability. However, in some cases such a distance independence can be an advantage for the systems where we can tune the rate of formation and recombination of the ^{1}(TT) independently. Our work therefore provides a fundamental insight into the SF mechanism where the multiexcitonic state can be stabilized in a dimeric system although the monomer doesn't meet the thermodynamic criteria for SF.

Electronic structure calculations

The NDI monomer and dimer geometries were optimized at the B3LYP/6-31G level of theory using Gaussian software.[28,29] Using the above methodology we optimized three dimeric structures: *Cyclo-Cyclo*, *Meta-Meta*, and *Ortho-Meta*. In all the dimer optimized structures, the monomers are no longer planar, they become contorted (Fig. S37). The excited state energies are calculated using a state average complete active space self-consistent field (SA-CASSCF) along with *n*-electron valence state perturbation theory (NEVPT2) with a cc-pVDZ basis as shown in Table 1 (details in the SI). We computed the excited state energies of the dimers, and the relevant couplings between the states. The electronic coupling between two non-adiabatic states can be determined as $\langle\psi_i|H_{el}|\psi_f\rangle$, where ψ_i and ψ_f are two non-adiabatic states and H_{el} is the electronic Hamiltonian. Here, the molecular orbitals used for the coupling calculations are obtained from the (4e, 4o) CASSCF calculations followed by localization. The expression of each of the coupling terms is taken from the papers Berkelbach *et al.* and Santra *et al.*[30–32]

We calculate the excitation energies of the dimers and ascertain the presence of low-lying ^{1}(TT) states. The energies of the low-lying states are given in Table S8, and we observe that all the states have mixed character due to the proximity of the monomers. The characters of each state and their CASSCF energies are given in the SI (Table S8). In order to elucidate the thermodynamics of the SF process we computed the singlet and triplet states in the monomer and observed that they do not satisfy the thermodynamic energy criterion for SF. Therefore, the reason behind this apparent violation of the energy rules of SF is further investigated. The possible reasons could be geometric contortions from the monomer system or strong coupling between monomers. We have calculated the low-lying excited state energies of contorted monomers and found that contortion is not the leading cause for SF (Table S4). The effects of deformation on the low-lying energy gaps of π-conjugated systems are known to be somewhat minimal.[33] Therefore, in line with these findings, we observe that the geometric twist on the monomers does not lead to a significant effect on the energetics.

The increasing distance between the two monomers widens the energy gap between the first excited ^{1}(TT) pair state and the other excited states (shown in Fig. S38). This increase reduces

Table 1 Five excited state (ES) energies of all three dimers in eV using the 6SA-CASSCF (4e, 4o)/NEVPT2/cc-pVDZ level of theory

ES	*Cyclo-Cyclo* (eV)	*Meta-Meta* (eV)	*Ortho-Meta* (eV)
S_1	1.65	2.17	1.94
S_2	1.65	2.21	2.02
S_3	2.17	2.90	2.25
S_4	2.24	3.29	2.86
S_5	3.59	3.72	3.37

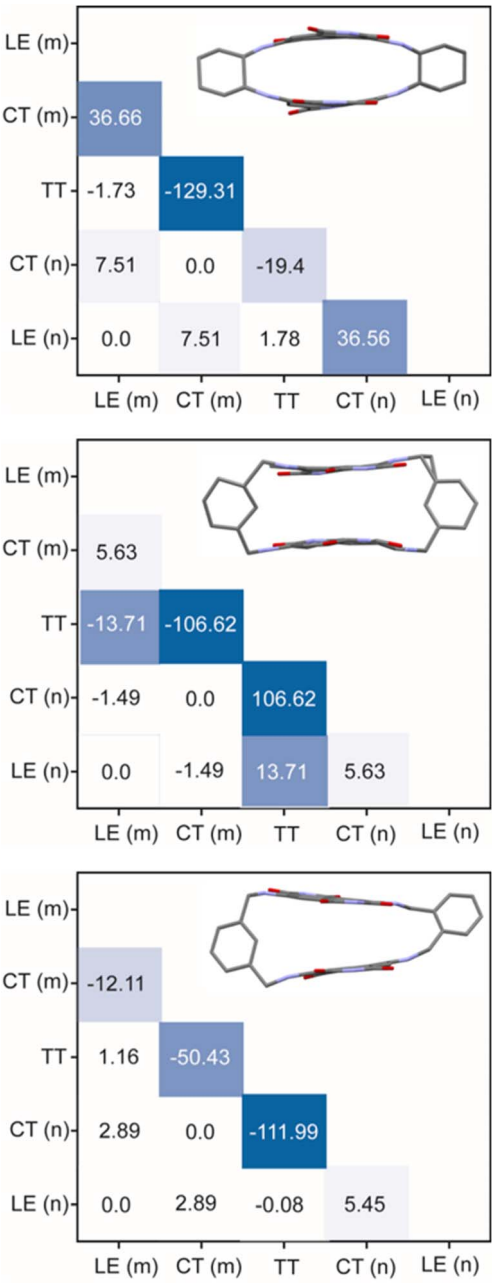

Fig. 6 The off-diagonal terms of the electronic coupling matrices are presented for *Cyclo-Cyclo*, *Meta-Meta* and *Ortho-Meta* (from top to bottom). Here *m* and *n* represent two monomers. LE(*m*) and LE(*n*) denote local excitations on monomers *m* and *n*, respectively. Similarly, CT(*m*) indicates charge transfer from monomer *m* to *n* and CT(*n*) indicates charge transfer from *n* to *m*.

the likelihood of energy transfer to the ^{1}(TT) pair state. A similar trend is observed from the couplings between the states of the three dimers. The coupling values are calculated following the method described by Berkelbach *et al.* and Santra *et al.*[30–32] and are depicted in Fig. 6. Based on the inter-chromophoric distance, the three dimers can be ranked in ascending order as *Cyclo-Cyclo*, *Ortho-Meta* and *Meta-Meta*. With the smallest interchromophoric distance, *Cyclo-Cyclo* exhibits efficient coupling for energy transfer from LE to ^{1}(TT) *via* a CT state. *Ortho-Meta* shows slightly lower energy transfer efficiency while *Meta-Meta* exhibits significantly lower energy transfer efficiency. It should be noted here that all the dimers show quenched emission with a slightly red-shifted feature with respect to the monomer emission spectral feature. Thus, interchromophoric interaction plays a crucial role in stabilization of the ^{1}(TT) pair state thereby establishing firmly the trends observed in the experimental SF rates. To investigate the relationship between ^{1}(TT) state recombination and interchromophoric distance, we carried out geometry optimization of the first excited state for Cyclo-Cyclo, *Ortho-Meta* and *Meta-Meta* dimers using the B3LYP/6-31G level of theory. At the optimized geometries, we evaluated the interchromophoric distances, defined as the center-of-mass separation between the monomeric units within each dimer. The calculated distances for the three systems are summarized in Table S2 and S3. Interestingly, our analysis reveals that there is no straightforward correlation between the recombination time of the correlated ^{1}(TT) pair state and the interchromophoric separation as we move from *Cyclo-Cyclo* to *Ortho-Meta* to *Meta-Meta*. This suggests that additional factors beyond mere spatial proximity may significantly influence the recombination dynamics of the ^{1}(TT) state.

Additionally, such quenched emission and geometrically stabilized ^{1}(TT) state clearly distinguishes itself from a potential excimer state. Interestingly, our computational efforts indicate that an interchromophoric distance of >5 Å may lead to inhibition of SF in these NDI dimers (Fig. S38). Overall, we realize that the stabilization of the ^{1}(TT) pair state on a dimeric framework is the most important criterion for singlet exciton fission.

Conclusion

In summary, here we provide the first systematic modulation of singlet fission rates for chromophoric dimers where the monomer does not satisfy the conventional SF singlet–triplet energy criteria. We examined a series of covalently linked NDI chromophoric cyclophanes with systematically varied linker lengths and electronic coupling (>100 meV) while probing the rates of ^{1}(TT) pair formation. We observe strong correlation of the rate of ^{1}(TT) formation with the inter-chromophoric distance, reflecting the diminishing electronic coupling strength across the series. Interestingly, comparing between the symmetric dimers, we find an increasing inter-chromophoric distance from the Cyclo-Cyclo dimer (∼3.3 Å) to the *Meta-Meta* dimer (∼4.5 Å). The distance correlation suggests a short-range interaction of order $\sim r^{-12}$ dictates the SF rates. This clearly hints at the repulsive interactions that distort the NDI chromophores in the dimer at the shortest distance of 3.3 Å. Similarly, for the symmetric dimers, the ^{1}(TT) pair recombination timescale was significantly extended in the *Meta-Meta* dimer to 115 ps relative to the *Cyclo-Cyclo* dimer having a 70 ps recombination timescale. This can be attributed to the weak electronic coupling in the *Meta-Meta* dimer (107 meV), which facilitates the formation of a relaxed correlated ^{1}(T⋯T) pair state.

However, for the unsymmetric dimers, the recombination rate showed no clear correlation with the ground-state interchromophoric distance or orientation, suggesting a reorganization or altered excited state geometry in the ^{1}(TT) state. This weak dependence offers an advantage for designing systems where the rates of ^{1}(TT) formation and recombination can be tuned independently. Therefore, our work highlights that cyclophanes, by virtue of their rigid and well-defined conformational architecture, offer superior control over the geometry to host the triplet pair state compared to more flexible, open dimers. We thus propose the design of a universal dimer system that can enable SF even with chromophores that do not strictly satisfy the energetic requirements for triplet formation, potentially opening new avenues for triplet harvesting and charge separation at donor–acceptor interfaces.

Author contributions

P. M. and J. D. conceived the idea of testing SF rates as a function of interchromophoric distance and angle. V. P. S. with help from P. M. synthesized the molecular dimers. A. M. performed the steady state absorption, emission along with all the time-resolved measurements. A. M. and J. D. analyzed the spectroscopic data. V. P. S. and Ch. M. H. carried out single crystal X-ray crystallography and electrochemical experiments. M. D. carried out all the theoretical calculations with methods and computational inputs provided by D. G. The manuscript was written by J. D., A. M., P. M., V. P. S., Ch. M. H., D. G., and M. D. The overall discussion and manuscript content was directed by J. D., D. G., and P. M. All the authors agreed to the final version of the manuscript.

Conflicts of interest

There are no conflicts to declare.

Data availability

The data supporting this article have been included as part of the supplementary information (SI). Supplementary information: description of the materials and experimental methods, additional figures pertaining to the experiments. See DOI: **https://doi.org/10.1039/d5sc05995j**.

CCDC 2424208 (*Ortho-Meta*) and 2424209 (*Meta-Meta*) contain the supplementary crystallographic data for this paper.[34a,b]

Acknowledgements

A. M. and J. D. acknowledge support from the Department of Atomic Energy (DAE), Government of India, under Project no. 12 R&D-TFR-5.10-0100. P. M. acknowledges SERB grant no. CRG/2021/008494 for partial funding. P. M. thanks Dr Deepak Bansal for his valuable initial inputs on the synthesis of the NDI dimers. D. G. is thankful for the generous funding from the SERB-POWER fellowship and IACS computational facilities. We thank AIRF, JNU for the instrumentation facilities and DST-FIST for the single crystal X-ray facility at SPS, JNU. We thank Geetanjali Dhotre (TIFR Mumbai) for TCSPC measurements and the National NMR facility (TIFR Mumbai) for characterization. The authors thank Professor Ayan Datta and Dr Arun Pal (IACS Kolkata) for many extensive discussions and being part of a collaboration. Additionally, the authors acknowledge Dr Arup Kundu (MIT) for initiating the discussions on the collaborative project on singlet fission in NDI

Notes and references

1 M. B. Smith and J. Michl, Recent Advances in Singlet Fission, *Annu. Rev. Phys. Chem.*, 2013, **64**(64), 361–386.
2 M. B. Smith and J. Michl, Singlet Fission, *Chem. Rev.*, 2010, **110**(11), 6891–6936.
3 S. Singh, W. J. Jones, W. Siebrand, B. P. Stoicheff and W. G. Schneider, Laser Generation of Excitons and Fluorescence in Anthracene Crystals, *J. Chem. Phys.*, 1965, **42**, 330–342.
4 W. Shockley and H. J. Queisser, Detailed Balance Limit of Efficiency of p-n Junction Solar Cells, *J. Appl. Phys.*, 1961, **32**(3), 510–519.
5 M. C. Hanna and A. J. Nozik, Solar conversion efficiency of photovoltaic and photoelectrolysis cells with carrier multiplication absorbers, *J. Appl. Phys.*, 2006, **100**(7), 074510.
6 M. Einzinger, T. Wu, J. F. Kompalla, H. L. Smith, C. F. Perkinson, L. Nienhaus, S. Wieghold, D. N. Congreve, A. Kahn, M. G. Bawendi and M. A. Baldo, Sensitization of silicon by singlet exciton fission in tetracene, *Nature*, 2019, **571**(7763), 90–94.
7 D. Chen, J. Shao, T. Zhang, K. Xu, C. Liang, Y. Cai, Y. Guo, P. Chen, X. Z. Mou and X. Dong, Aromaticity Tuning of Heavy-Atom-Free Photosensitizers for Singlet Fission-Enhanced Immunogenic Photodynamic Oncotherapy, *Nano Lett.*, 2024, **24**, 7524–7533.
8 I. Paci, J. C. Johnson, X. Chen, G. Rana, D. Popović, D. E. David, A. J. Nozik, M. A. Ratner and J. Michl, Singlet Fission for Dye-Sensitized Solar Cells: Can a Suitable Sensitizer Be Found?, *J. Am. Chem. Soc.*, 2006, **128**(51), 16546–16553.
9 A. Bhattacharyya, A. Sahu, S. Patra and V. Tiwari, Low- and high-frequency vibrations synergistically enhance singlet exciton fission through robust vibronic resonances, *Proc. Natl. Acad. Sci. U. S. A.*, 2023, **120**(49), e2310124120.
10 H. Liu, X. Wang, L. Ma, W. Wang, S. Liu, J. Zhou, P. Su, Z. Liu, Z. Li, X. Lin, Y. Chen and X. Li, Effects of the Separation Distance between Two Triplet States Produced from Intramolecular Singlet Fission on the Two-Electron-Transfer Process, *J. Am. Chem. Soc.*, 2022, **144**(34), 15509–15518.
11 N. Monahan and X.-Y. Zhu, Charge Transfer–Mediated Singlet Fission, *Annu. Rev. Phys. Chem.*, 2015, **66**(66), 601–618.
12 E. G. Fuemmeler, S. N. Sanders, A. B. Pun, E. Kumarasamy, T. Zeng, K. Miyata, M. L. Steigerwald, X. Y. Zhu, M. Y. Sfeir, L. M. Campos and N. Ananth, A Direct Mechanism of Ultrafast Intramolecular Singlet Fission in Pentacene Dimers, *ACS Cent. Sci.*, 2016, **2**(5), 316–324.
13 J. Kim, H. T. Teo, Y. Hong, H. Cha, W. Kim, C. Chi and D. Kim, Elucidating Singlet-Fission-Born Multiexciton Dynamics via Molecular Engineering: A Dilution Principle Extended to Quintet Triplet Pair, *J. Am. Chem. Soc.*, 2024, **146**(15), 10833–10846.
14 J. Zirzlmeier, D. Lehnherr, P. B. Coto, E. T. Chernick, R. Casillas, B. S. Basel, M. Thoss, R. R. Tykwinski and D. M. Guldi, Singlet fission in pentacene dimers, *Proc. Natl. Acad. Sci. U. S. A.*, 2015, **112**(17), 5325–5330.
15 A. Mandal, M. Chen, E. D. Foszcz, J. D. Schultz, N. M. Kearns, R. M. Young, M. T. Zanni and M. R. Wasielewski, Two-Dimensional Electronic Spectroscopy Reveals Excitation Energy-Dependent State Mixing during Singlet Fission in a Terrylenediimide Dimer, *J. Am. Chem. Soc.*, 2018, **140**(51), 17907–17914.
16 S. N. Sanders, E. Kumarasamy, A. B. Pun, M. T. Trinh, B. Choi, J. Xia, E. J. Taffet, J. Z. Low, J. R. Miller, X. Roy, X. Y. Zhu, M. L. Steigerwald, M. Y. Sfeir and L. M. Campos, Quantitative Intramolecular Singlet Fission in Bipentacenes, *J. Am. Chem. Soc.*, 2015, **137**(28), 8965–8972.
17 S. Khan and S. Mazumdar, Free Triplets Versus Bound Triplet–Triplet Biexciton in Intramolecular Singlet Fission Materials: Structure–Property Correlations, *J. Phys. Chem. C*, 2020, **124**(1), 1171–1177.
18 N. V. Korovina, J. Joy, X. Feng, C. Feltenberger, A. I. Krylov, S. E. Bradforth and M. E. Thompson, Linker-Dependent Singlet Fission in Tetracene Dimers, *J. Am. Chem. Soc.*, 2018, **140**(32), 10179–10190.
19 J. Choi, S. Kim, M. Ahn, J. Kim, D. W. Cho, D. Kim, S. Eom, D. Im, Y. Kim, S. H. Kim, K.-R. Wee and H. Ihee, Singlet fission dynamics modulated by molecular configuration in covalently linked pyrene dimers, Anti- and Syn-1,2-di(pyrenyl)benzene, *Commun. Chem.*, 2023, **6**(1), 16.
20 W. Kim, N. A. Panjwani, K. C. Krishnapriya, K. Majumder, J. Dasgupta, R. Bittl, S. Patil and A. J. Musser, Heterogeneous singlet fission in a covalently linked pentacene dimer, *Cell Rep. Phys. Sci.*, 2024, **5**(7), 102045.
21 K. Majumder, S. Mukherjee, N. A. Panjwani, J. Lee, R. Bittl, W. Kim, S. Patil and A. J. Musser, Controlling Intramolecular Singlet Fission Dynamics via Torsional Modulation of Through-Bond versus Through-Space Couplings, *J. Am. Chem. Soc.*, 2023, **145**(38), 20883–20896.
22 H. M. Bergman, G. R. Kiel, R. J. Witzke, D. P. Nenon, A. M. Schwartzberg, Y. Liu and T. D. Tilley, Shape-Selective Synthesis of Pentacene Macrocycles and the Effect of

Geometry on Singlet Fission, *J. Am. Chem. Soc.*, 2020, **142**(47), 19850–19855.

23 W. Ishii, M. Fuki, E. M. Bu Ali, S. Sato, B. Parmar, A. Yamauchi, C. H. Mulyadi, M. Uji, S. Medina Rivero, G. Watanabe, J. Clark, Y. Kobori and N. Yanai, Macrocyclic Parallel Dimer Showing Quantum Coherence of Quintet Multiexcitons at Room Temperature, *J. Am. Chem. Soc.*, 2024, **146**(37), 25527–25535.

24 D. Bansal, A. Kundu, V. P. Singh, A. K. Pal, A. Datta, J. Dasgupta and P. Mukhopadhyay, A highly contorted push–pull naphthalenediimide dimer and evidence of intramolecular singlet exciton fission, *Chem. Sci.*, 2022, **13**(39), 11506–11512.

25 L. Stryer and R. P. Haugland, Energy transfer: a spectroscopic ruler, *Proc. Natl. Acad. Sci. U. S. A.*, 1967, **58**(2), 719–726.

26 L. van Turnhout, D. G. Congrave, Z. Yu, R. Arul, S. A. Dowland, E. Sebastian, Z. Jiang, H. Bronstein and A. Rao, Distance-Independent Efficiency of Triplet Energy Transfer from π-Conjugated Organic Ligands to Lanthanide-Doped Nanoparticles, *J. Am. Chem. Soc.*, 2024, **146**(32), 22612–22621.

27 S. M. Hart, W. R. Silva and R. R. Frontiera, Femtosecond stimulated Raman evidence for charge-transfer character in pentacene singlet fission, *Chem. Sci.*, 2018, **9**(5), 1242–1250.

28 M. J. Frisch, G. W. Trucks, H. B. Schlegel, *et.al.*, *Gaussian 16*, Rev. C.01, 2016.

29 M. J. Frisch, G. W. Trucks, H. B. Schlegel, G. E. Scuseria, M. A. Robb, J. R. Cheeseman, G. Scalmani, V. Barone, G. A. Petersson, H. Nakatsuji, X. Li, M. Caricato, A. V. Marenich, J. Bloino, B. G. Janesko, R. Gomperts, B. Mennucci, H. P. Hratchian, J. V. Ortiz, A. F. Izmaylov, J. L. Sonnenberg, Williams, F. Ding, F. Lipparini, F. Egidi, J. Goings, B. Peng, A. Petrone, T. Henderson, D. Ranasinghe, V. G. Zakrzewski, J. Gao, N. Rega, G. Zheng, W. Liang, M. Hada, M. Ehara, K. Toyota, R. Fukuda, J. Hasegawa, M. Ishida, T. Nakajima, Y. Honda, O. Kitao, H. Nakai, T. Vreven, K. Throssell, J. A. Montgomery Jr, J. E. Peralta, F. Ogliaro, M. J. Bearpark, J. J. Heyd, E. N. Brothers, K. N. Kudin, V. N. Staroverov, T. A. Keith, R. Kobayashi, J. Normand, K. Raghavachari, A. P. Rendell, J. C. Burant, S. S. Iyengar, J. Tomasi, M. Cossi, J. M. Millam, M. Klene, C. Adamo, R. Cammi, J. W. Ochterski, R. L. Martin, K. Morokuma, O. Farkas, J. B. Foresman and D. J. Fox, *Gaussian 16*, Rev. C.01, Wallingford, CT, 2016.

30 T. C. Berkelbach, M. S. Hybertsen and D. R. Reichman, Microscopic theory of singlet exciton fission. I. General formulation, *J. Chem. Phys.*, 2013, **138**, 114102.

31 T. C. Berkelbach, M. S. Hybertsen and D. R. Reichman, Microscopic theory of singlet exciton fission. II. Application to pentacene dimers and the role of superexchange, *J. Chem. Phys.*, 2013, **138**, 114103.

32 S. Santra, J. Ray and D. Ghosh, Mechanism of Singlet Fission in Carotenoids from a Polyene Model System, *The Journal of Physical Chemistry Letters*, 2022, **13**(29), 6800–6805.

33 J. E. Norton and K. N. Houk, Electronic Structures and Properties of Twisted Polyacenes, *J. Am. Chem. Soc.*, 2005, **127**(12), 4162–4163.

34 (*a*) CCDC 2424208: Experimental Crystal Structure Determination, 2025, DOI: **10.5517/ccdc.csd.cc2mcl8w**; (*b*) CCDC 2424209: Experimental Crystal Structure Determination, 2025, DOI: **10.5517/ccdc.csd.cc2mcl9x**.